CHINESE OPTICS LETTERS

Vol. 22, No. 5 | May 2024

Stability-enhanced RF signal transmission over long fiber-optic links

Zhiqian Yin (尹知谦)[1], Manhang Zheng (郑满航)[1], Chuanbo Zhang (张川博)[1], Shijian Guan (管世健)[1], Xin Zhou (周 昕)[1], Yitong Liu (刘奕彤)[1], Zeyu Gang (刚泽宇)[1], Jiaqiang Nie (聂佳强)[1], Yunshan Zhang (张云山)[2], Xingbang Zhu (朱兴邦)[3], Tao Fang (方 涛)[1*], and Xiangfei Chen (陈向飞)[1**]

[1] Engineering Research Center of Precision Photonics Integration and System Application, Ministry of Education & Key Laboratory of Intelligent Optical Sensing and Manipulation, Ministry of Education & National Laboratory of Solid State Microstructures & College of Engineering and Applied Sciences & Institute of Optical Communication Engineering & Nanjing University-Tongding Joint Lab for Large-scale Photonic Integrated Circuits, Nanjing University, Nanjing 210023, China

[2] College of Electronics and Optical Engineering and College of Flexible Electronics (Future Technology), Nanjing University of Posts and Telecommunications, Nanjing 210023, China

[3] The 41st Research Institute of China Electronics Technology Group Corp, Qingdao 266000, China

*Corresponding author: fangt@nju.edu.cn

**Corresponding author: chenxf@nju.edu.cn

Received December 4, 2023 | Accepted January 16, 2024 | Posted Online May 14, 2024

We propose a method for optimizing the phase stability of microwave signal transmission over long distances. First, the design of the photon link was modified to reduce the radio frequency (RF) signal's baseline noise and increase power. Second, a low-noise driver circuit was developed for a two-section distributed feedback (DFB) laser designed using reconstruction equivalent chirp (REC) technology to create an ultra-stable laser, and its performance was characterized through linewidth data. Test results indicate that the DFB laser achieved narrower linewidth, improving system phase stability. When an injection current (30 mA) is applied to the reflection section of the two-section DFB laser, the laser linewidth will be narrower (1.38 MHz), further enhancing the system's phase transmission stability. At a 1 Hz offset frequency, a residual phase noise of −88.65 dBc/Hz is obtained. The short-term stability with an averaging time of 1 s is 1.60×10^{-14}, and the long-term stability over a testing time of 60,000 s is 3.41×10^{-18}. Even after incorporating temperature variations, the long-term stability reaches 8.37×10^{-18} at 22 h.

Keywords: frequency dissemination; two-section distributed feedback laser; phase stability.
DOI: 10.3788/COL202422.053901

1. Introduction

With the continuous growth of modern society's demand for high-speed and high-precision communication and measurement, stability has become an indispensable and crucial concept across various technological fields[1,2]. In this context, phase stability system transmission, as a key technology ensuring the consistency and precision of signal phase, is increasingly gaining widespread attention and research[3]. From communication to science, navigation to healthcare, and precision measurement to cutting-edge research, phase stability system transmission is reshaping our understanding of information transmission and signal processing[4,5].

However, when transmitting microwave signals over long distances, the phase stability is often constrained by various factors, among which the most crucial are the design of the optical carrier emission module and the phase stability system, as well as the performance of the optical components used[6,7]. Optical components such as optical couplers, circulators, and fibers are used to guide and process optical signals. The stability, losses, and dispersion characteristics of these components can impact the transmission quality of optical signals and phase stability[8,9]. Proper selection and optimization of optical components can reduce signal loss, decrease dispersion effects, and thus ensure the performance of the phase stability system[10,11]. In this Letter, building upon the previously designed phase stability system, we optimized the design of the optical components used, which played a significant role in enhancing the system's stability. The laser is a core component of the phase stability system, and its output characteristics directly affect stable phase transmission. Parameters like laser linewidth, frequency stability, and output power influence the phase noise characteristics of the

system[12-16]. Choosing a laser with lower linewidth and frequency drift can improve the phase stability of the system. In prior work, we found that a two-section DFB analog direct modulation laser (DML) designed using REC technology could improve the system's phase transmission stability by injecting current into the DML reflection section (RS)[17,18]. In this article, we delve into the impact of changing the power supply scheme to the RS of the analog DML on the output wavelength linewidth, as well as its effects on the overall phase stability of the system. The stability and precision of the driver circuit, which controls the laser's operation, directly affect the laser's output characteristics. A stable driver circuit can reduce the laser's frequency drift, thereby enhancing phase stability. Based on this, we designed a specialized laser driver circuit suitable for the phase stability system, aimed at providing a stable power supply and temperature control for DML.

In this paper, we have optimized the arrangement of the phase stability transmission system by focusing on the system's DML, its driver circuit, and the optical instruments employed. Through these optimizations, we have achieved an enhancement in the stability of the transmitted RF signals over a 50 km fiber link. The study provides the optimized power-current (*P-I*) curve and 3 dB modulation bandwidth of the analog DML. The feasibility of the designed ultra-stable driver circuit was validated using linewidth data. Additionally, we analyzed the variations in output wavelength linewidth and spectral characteristics when different currents are applied to the RS of the analog DML. Finally, we conducted tests to examine the phase noise of the system and its stability under varying injection currents to the RS. To better adapt to industrial applications, we introduced temperature variations to the 50 km optical fiber spool to simulate real-world conditions and conducted stability tests accordingly.

2. Experimental Design

As shown in Fig. 1(a), the schematic diagram of the phase stability transmission system is nearly identical to the previous transmission system in terms of instrument arrangement[19]. In this paper, two modifications and optimizations were primarily carried out to reduce the optical power loss in the link and the effects of Brillouin scattering and backward Rayleigh scattering on system stability. Although the attenuation of light during transmission in optical fiber is already minimal, as the transmission distance increases, optical power loss also grows. Minimizing optical losses in the link is crucial, as it helps avoid the introduction of the EDFA, thereby reducing noise in the link. By changing the positions of the central site OC1 and the circulator, secondary power distribution on the OC1 due to the returning optical signal was avoided, leading to an increase in the optical power entering PD_3. Furthermore, integrating the OC1 and circulator into a single optical module circumvents connector losses between them, further reducing optical power loss in the link.

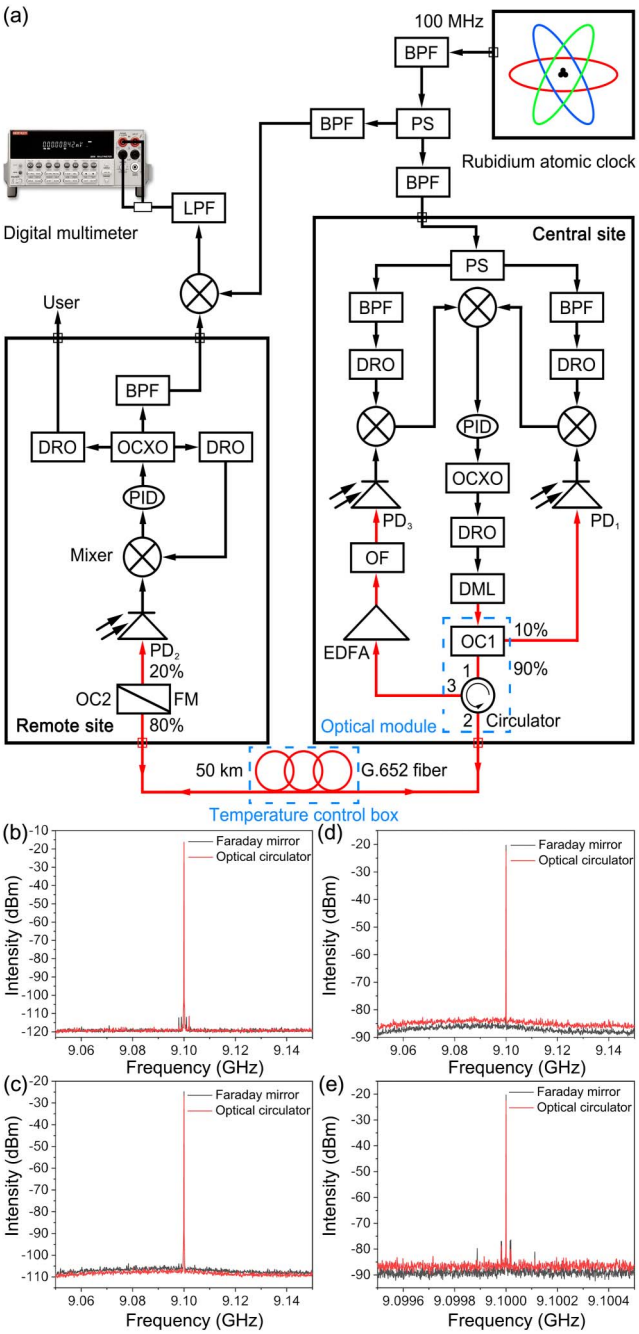

Fig. 1. (a) The working principle of phase stability transmission system. BPF: bandpass filter; PS: power splitter; DRO: dielectric resonant oscillator; OCXO: oven-controlled crystal oscillator; PID: proportional-integral-differential; OC: optical coupler; PD: photodetector; EDFA: erbium-doped fiber amplifier; OF: optical filter; LPF: low-pass filter; FM: Faraday mirror. (b)–(d) The signal and spectrum analyzer observes the demodulated RF signals from PD_1, PD_2, and PD_3 (black: remote site internally employs OC2 and an FM; red: remote site internally uses OC2 and an optical circulator). (e) Observed demodulated RF signal from PD_3 under a narrower frequency range.

To overcome the effects of dispersion caused by round-trip delays in dual-wavelength systems, single-wavelength transmission was employed to mitigate the asymmetry issue brought

about by the round-trip link. The impact of Rayleigh scattering on single-wavelength frequency signal transfer systems is mainly twofold. On one hand, Rayleigh scattering of the forward signal interferes with the return signal. The return signal is used for pre-compensation processing at the central site, resulting in the Rayleigh scattering signal eventually affecting the compensated signal and degrading the compensation accuracy of the frequency transfer system. On the other hand, Rayleigh scattering of the backward signal is directly received by the PD. The phase and amplitude disturbances introduced by Rayleigh noise cause a reduction in signal quality, subsequently lowering the signal-to-noise ratio and overall transmission quality. The arrangement of the OC1 before the circulator ensures that the optical power leaving the circulator's second port is only 90% of the optical power coming out of the DML. This also mitigates the impact of backward Rayleigh scattering on PD_3. At the remote site, the combination of an OC2 and an FM replaced the combination of an OC2 and a circulator[20-22]. The use of an FM introduces a 45° phase shift to the optical signal transmission. The signal reflected by the FM exhibits a 90° phase difference compared to the incident signal, thus placing the phase of the returned signal orthogonal onto that of the forward signal. Additionally, integrating the OC2 and the FM into a single device significantly reduces the volume and eliminates connector losses between the devices.

The previous combination of the OC2 and the circulator formed a loop at the remote site, which caused the continuous accumulation of backward Rayleigh scattering and increased the transmission distance, amplifying the impact of stimulated Brillouin scattering. The combination of the OC2 and the FM, however, breaks this loop, resulting in gains in the strength and quality of the transmitted signal. Figures 1(b)–1(d) present the demodulation conditions of PD_1, PD_2, and PD_3 when using the integrated OC1 and circulator at the central site, the combination of the OC2 and the FM at the remote site, and the combination of the OC2 and the circulator at the remote site. From Fig. 1(b), it can be observed that, although PD_1's demodulated optical signal exhibits MHz-level harmonics, the signal-to-noise ratio reaches 95 dB, which has little impact on stability and can be neglected. From the demodulation results for PD_2 in Fig. 1(c), the optimization effect of the FM is not prominent. However, the demodulated signal possesses a high signal-to-noise ratio and lacks excess harmonics, thereby having a minor influence on the final stability result. The signal demodulated by PD_3 is more severely affected, as the optical signal has traveled the 50 km transmission link twice, experiencing attenuation, dispersion, and the more pronounced influence of stimulated Brillouin scattering. Figure 1(d) clearly shows that using the FM instead of the circulator significantly reduces the bottom noise of the RF signal. Figure 1(e) narrows the observation range from Fig. 1(d), reducing bottom noise by approximately 3 dB and raising the signal-to-noise ratio from 66.61 dB to 69.65 dB. In Fig. 1(e), 10-kHz-level harmonics can be observed, with a signal-to-noise ratio of approximately 56 dB, which essentially satisfies the stability test requirements of the system. In summary, the changes to the system have optimized the transmission quality of the RF signal.

3. Results and Discussion

As shown in Fig. 2(a), the designed two-section analog DML is almost identical in manufacturing details to the previously designed laser[23]. To enhance the DML slope efficiency, adjustments were made to the DML cavity length. The cavity length of the previous LS was changed from 400 μm to 350 μm, and the cavity length of the RS was reduced from 600 μm to 450 μm. The laser's cavity length determines both the slope efficiency of the laser and the output optical power, both of which are critical factors in the phase stability transmission system. At the same bias current, a laser with higher slope efficiency has a deeper modulation depth. A higher slope efficiency not only ensures a higher modulation depth at low currents but also avoids stimulated Brillouin scattering at high currents. High slope efficiency lasers generate higher output power, increasing the signal-to-noise ratio of the transmitted signal and reducing the impact of phase

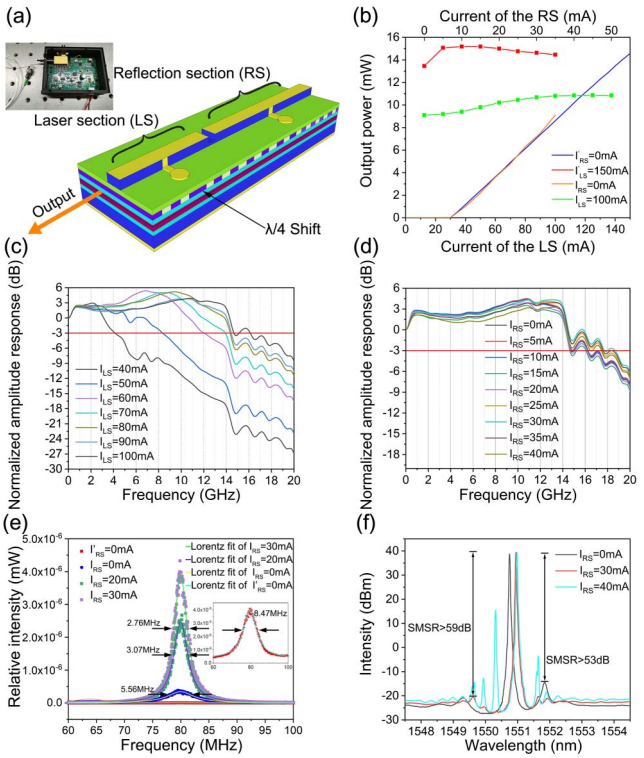

Fig. 2. (a) Schematic of two-section analog DML; the inset is a picture of the analog DML chip after packaging and in use. (b) Comparison between the *P-I* curve of the adjusted two-section analog DML and the previous analog DML. (c) Modulation amplitude response of the two-section analog DML when I_{RS} = 0 mA. (d) Modulation amplitude response of the two-section analog DML when I_{LS} = 100 mA. (e) Lorentzian fitting for 3 dB linewidth when I_{RS} = 0, 20, 30 mA and I'_{RS} = 0 mA; the inset is an enlargement of the linewidth fitting results when I'_{RS} = 0 mA. (f) Laser spectra when I_{RS} is set to 0, 30, and 40 mA.

noise. Additionally, in the low-current operating state of the laser, the thermoelectric cooler (TEC) on the driver circuit board can better control the laser's temperature, maintaining its stable operation and improving signal quality and system performance. The inset in Fig. 2(a) depicts the integrated DML and the designed ultra-stable drive control circuit, utilizing a high-precision TEC for laser temperature control. The ultra-stable driver circuit, with lower current fluctuations and more stable temperature control, ensures lower noise for the DML during operation. Figure 2(b) presents the *P-I* curves of the DML after changing the cavity lengths of the LS and RS, as well as the *P-I* curves of the previously used laser. The description of the *P-I* curves for the previous laser has been elaborated in a previous article. Here, the orange line represents the case where the current of the RS is 0 mA, and the current of the LS continuously changes. The green line represents the case where the current of the LS is 100 mA, and the current of the RS continuously changes. The threshold currents of the two lasers are the same. As the phase stability system does not require excessively high optical power, only the power variation at an injection of 100 mA is tested. The objective of increasing slope efficiency was achieved by altering the cavity length. For injection currents greater than 75 mA, the optical power for equivalent current injection exceeded that of the previously used laser. Similarly to before, when the RS has no current, the feedback effect of the RS is weak due to absorption loss. With a small injection current, feedback is enhanced, leading to a significant increase in DML output power. As the injection current continues to increase, the DML output optical power does not saturate. Figures 2(c) and 2(d) show the modulation bandwidth of the optimized DML, tested using a vector network analyzer. From Fig. 2(c), it can be seen that despite shortening the DML cavity length, the LS can transmit an RF signal with a bandwidth of 9 GHz for injection currents greater than 50 mA, meeting the system's transmission requirements. Figure 2(d) displays the modulation bandwidth corresponding to different injection currents of the RS when the injection current of the LS is set to 100 mA. With the continuous increase of the RS current, the modulation bandwidth significantly expands.

Figure 2(e) shows the spectrum of the DML linewidth tested using the self-heterodyne method, along with the Lorentz curve fitting. Linewidth data were used to validate the feasibility of the ultra-stable driver circuit because the operating temperature of the laser and its stability can affect the laser's linewidth. A narrower laser linewidth indicates that the ultra-stable driver circuit can ensure the laser's stable operating temperature and lower current fluctuations. The linewidth of the DML was tested for injection currents of 100 mA in the LS and 0 mA, 20 mA, and 30 mA in the RS. I_{RS} represents the current value injected into the RS using the conventional driver circuit before optimization. The test spectral range was 40 MHz, the resolution was 1 MHz, the testing environment was 25°C, and the linewidth of the laser was represented by the full width at half-maximum (FWHM). As the measured spectral line was a Lorentzian line shape, using a Lorentzian fit would yield more accurate linewidth results. When the RS had no current injection, the FWHM of the beat signal was 5.56 MHz at 80 MHz, corresponding to a laser linewidth of 2.78 MHz after Lorentzian fitting. When the laser was injected with 100 mA current into LS and no current into RS using the conventional driver circuit, the linewidth significantly increased. It can be seen from the inset that the linewidth after the Lorentzian fitting was 4.24 MHz. This indicates that the designed driver circuit is capable of making the laser operate more stably. Interestingly, as the injection current of the RS increased, the DML linewidth gradually decreased. With injection currents of 20 mA and 30 mA in the RS, the linewidths after Lorentzian fitting were 1.54 MHz and 1.38 MHz, respectively. When the laser power is not saturated, the linewidth of a DFB laser is inversely proportional to the output optical power. This is per the theoretical expectations. Figure 2(f) illustrates the observation of the single-mode characteristics of the laser during linewidth testing. It can be seen that, as the injection current to the RS increases, the laser maintains a stable single longitudinal mode output. Simultaneously, the side mode suppression ratio (SMSR) of the spectrum improves, increasing from 53 dB at $I_{RS} = 0$ mA to 59 dB at $I_{RS} = 30$ mA. It is worth noting that, during the testing process, as the injection current to the RS increases from 30 mA to 40 mA, the laser linewidth continues to decrease. At this point, observing the spectrum reveals that the laser can no longer guarantee single-mode output, as multiple side modes appear, leading to inaccurate linewidth data.

Figure 3(a) illustrates the phase fluctuations of the transmission system under different conditions. The method for calculating phase fluctuations has been extensively described in previous articles[19]. The black line represents the signal's

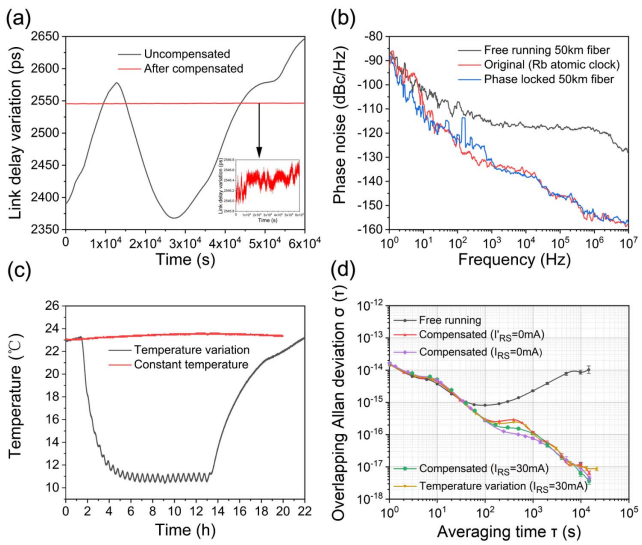

Fig. 3. (a) 50 km fiber link delay variation before and after compensation. (b) Phase noise of the frequency signal through 50 km fiber link (red: original rubidium atomic clock; black: free running; blue: phase-locked). (c) Temperature variation inside the temperature control box (red: constant temperature; black: variable temperature). (d) Preliminary fractional frequency stability of the 50 km free running link (black line), compensated link at 100 MHz when $I'_{RS} = 0$ mA (red line), 30 mA (green line), and $I_{RS} = 0$ mA (purple line), and compensated link during temperature fluctuations (golden line).

phase fluctuation during free transmission over a 50 km link, exhibiting a delay variation of about 280 ps over a testing time of 60,000 s. In contrast, the red line indicates the phase jitter of the signal after compensation by the system, with a delay variation of only 0.97 ps over the same 60,000 s testing time. In Fig. 3(b), phase noise tests were conducted for the rubidium atomic clock, free transmission, and system-compensated signals. The red line represents the high-performance rubidium atomic clock, demonstrating favorable phase noise characteristics at both low and high frequencies, measured as −92.49 dBc/Hz at 1 Hz and −157.47 dBc/Hz at 10 MHz, respectively. However, after undergoing 50 km transmission, the phase noise significantly deteriorated across the entire frequency offset range. This degradation is attributed to environmental changes in temperature, pressure, humidity, and impact of nonlinear optical effects. The blue line represents the phase noise of the signal for user utilization after compensation, showcasing excellent signal quality restoration, even surpassing the phase noise of the rubidium atomic clock at low frequencies. This result is due to the utilization of OCXO and DRO for signal restoration at the remote site, both of which have inherently high phase noise characteristics. Notably, a distinct peak is observed near a few hundred hertz, arising from the system's control loop bandwidth. To better simulate real-world scenarios, temperature changes were introduced to the transmission chain by placing the 50 km fiber spool inside a temperature control box. Figure 3(c) depicts the temperature variations experienced by the fiber spool. The red line represents temperature variations under constant conditions, with a minimal temperature change of 0.63°C within 20 h. Under variable temperature conditions, the transmission link first experienced rapid temperature reduction, followed by a gradual increase to simulate multiple temperature changes occurring in a day. Within 22 hours, the temperature fluctuated by 12.81°C, with a peak temperature of 23.31°C and a minimum temperature of 10.5°C. For buried optical fibers, temperature stability is relatively high compared to surface conditions, resulting in minor temperature fluctuations. Considering the depth of fiber burial, if the optical fiber is buried shallowly (<15 m), temperature changes usually fall within a few to a dozen degrees Celsius. In contrast, for optical fibers buried deeply (>20 m), temperature variations are relatively small, typically within a few degrees Celsius. Thus, the provided temperature variations are sufficient to simulate normal operating conditions for buried optical fibers. Figure 3(d) presents phase stability measured through the direct mixing method, illustrating the results for free transmission, varying injection currents into the DML RS, and temperature variations. When the injection current into the LS is set to 100 mA while the RS remains current-free, the stability improves by three orders of magnitude compared to free transmission, achieving a stability of 6.4×10^{-18} over a testing time of 60,000 s. After using the ultra-stable driving circuit, the signal transmission stability is further improved to 4.4×10^{-18}, indicating that reducing laser noise can indeed improve the phase transmission stability of the entire system. With an injection current of 30 mA into the RS, stability improves to 3.4×10^{-18}. This shows that the reduction of linewidth will reduce the impact of dispersion deterioration on stability, and the injection of current in the RS will also correspondingly increase the DML output power. Moreover, the injection current into the RS does not seem to significantly affect short-term stability, regardless of the current magnitude. The stability values remain around 1.5×10^{-14} s^{-1} to 1.6×10^{-14} s^{-1}, emphasizing that the impacts on signals during long-term transmission are more prominent. Finally, the stability under the conditions of injecting 100 mA into the LS and 30 mA into the RS under temperature variation is tested. Due to the multiple temperature changes, the stability worsens significantly. After testing for 86,000 s, the stability stabilizes at 8.3×10^{-18}. In conclusion, the ultra-stable laser can provide higher phase stability, frequency accuracy, and signal quality in phase-stable transmission systems, making them well-suited for applications requiring high precision, stability, and accuracy.

4. Conclusion

In this paper, an ultra-stable laser driver circuit is designed to improve the phase stability of the transmission system. First, we optimized the arrangement of the transmission system to increase the optical power while reducing the adverse effects of Rayleigh scattering and stimulated Brillouin scattering on system stability. Second, by shortening the cavity lengths of both sections of the DML, we enhanced the DML slope efficiency and characterized its modulation bandwidth. The 1.38 MHz linewidth shows that the ultra-stable driver circuit can provide a more stable working state for the laser. Lastly, the results of the phase stability also show that ultra-stable DML helps improve the phase transmission stability of the system. When the RS was driven at 30 mA, the phase stability achieved over a test duration of 60,000 s was 3.4×10^{-18}. Even after subjecting the transmission link to repeated temperature variations of up to 13°C, the phase stability remained at 8.3×10^{-18} after a test duration of 86,000 s. In conclusion, we used an ultra-stable two-section analog DML to enhance the stability of a transmission system. Furthermore, our phase-stable transmission system demonstrates great potential for practical real-life applications.

Acknowledgements

This work was supported by the National Key R&D Program of China (No. 2020YFB2205804) and the National Natural Science Foundation of China (Nos. 62273355, 62374092, 61975075, 61975076, and 62004094).

References

1. D. Hou, P. Li, P. Xi, *et al.*, "Timing jitter reduction over 20-km urban fiber by compensating harmonic phase difference of locked femtosecond comb," Chin. Opt. Lett. **8**, 993 (2010).
2. F. F. Yin, A. X. Zhang, Y. T. Dai, *et al.*, "Phase-conjugation-based fast RF phase stabilization for fiber delivery," Opt. Express **22**, 878 (2014).

3. L. S. Ma, P. Jungner, J. Ye, *et al.*, "Delivering the same optical frequency at two places: accurate cancellation of phase noise introduced by an optical fiber or other time-varying path," Opt. Lett. **19**, 1777 (1994).
4. K. W. Holman, D. D. Hudson, J. Ye, *et al.*, "Remote transfer of a high-stability and ultralow-jitter timing signal," Opt. Lett. **30**, 1225 (2005).
5. M. Kumagai, M. Fujieda, S. Nagano, *et al.*, "Stable radio frequency transfer in 114 km urban optical fiber link," Opt. Lett. **34**, 2949 (2009).
6. G. Marra, R. Slavík, H. S. Margolis, *et al.*, "High-resolution microwave frequency transfer over an 86-km-long optical fiber network using a mode-locked laser," Opt. Lett. **36**, 511 (2011).
7. L. M. Zhang, L. Chang, Y. Dong, *et al.*, "Phase drift cancellation of remote radio frequency transfer using an optoelectronic delay-locked loop," Opt. Lett. **36**, 873 (2011).
8. S. M. Foreman, A. D. Ludlow, M. H. G. D. Miranda, *et al.*, "Coherent optical phase transfer over a 32-km fiber with 1 s instability at 10^{-17}," Phys. Rev. Lett. **99**, 153601 (2007).
9. P. Krehlik, Ł. Buczek, J. Kołodziej, *et al.*, "Fibre-optic delivery of time and frequency to VLBI station," Astron. Astrophys. **603**, A48 (2017).
10. P. Krehlik, H. Schnatz, and Ł. Śliwczyński, "A hybrid solution for simultaneous transfer of ultrastable optical frequency, RF frequency, and UTC time-tags over optical fiber," IEEE Trans. Sonics Ultrason. **64**, 1884 (2017).
11. S. M. Foreman, K. W. Holman, D. D. Hudson, *et al.*, "Remote transfer of ultrastable frequency references via fiber networks," Rev. Sci. Instrum. **78**, 021101 (2007).
12. J. X. B. Sia, X. Li, W. J. Wang, *et al.*, "Sub-kHz linewidth, hybrid III–V/silicon wavelength-tunable laser diode operating at the application-rich 1647–1690 nm," Opt. Express **28**, 5134 (2020).
13. Y. Wu, L. H. Deng, K. Y. Yang, *et al.*, "Narrow linewidth external cavity laser capable of high repetition frequency tuning for FMCW LiDAR," IEEE Photon. Technol. Lett. **34**, 1123 (2022).
14. H. Ishii, K. Kasaya, and H. Oohashi, "Spectral linewidth reduction in widely wavelength tunable DFB laser array," IEEE J. Sel. Top. Quantum Electron. **15**, 514 (2009).
15. D. D. Wang, Y. F. Jiang, H. Gu, *et al.*, "Improvement and analysis of a recirculating delayed self-heterodyne interferometer for laser linewidth measurement," Opt. Fiber Technol. **71**, 102945 (2022).
16. X. Li, L. Liang, L. Qin, *et al.*, "Development of a high-power surface grating tunable distributed-feedback Bragg semiconductor laser based on gain-coupling effect," Appl. Sci. **12**, 4498 (2022).
17. M. J. Chen, Y. C. Shi, R. L. Xiao, *et al.*, "Tunable DFB laser array for multi-gas detection," in *19th International Conference on Optical Communications and Networks* (2021), p. 1.
18. Y. S. Zhang, Y. Liu, J. Lu, *et al.*, "DFB laser arrays based on the REC technique and their applications in radio-over-fiber systems (Invited Paper)," Chin. Opt. Lett. **15**, 010005 (2017).
19. Z. Yin, C. Zhang, S. Guan, *et al.*, "Long-term ultrastable frequency dissemination via a 50-km spooled fiber link using a two-section DFB laser," Chin. Opt. Lett. **22**, 013903 (2024).
20. P. A. Williams, W. C. Swann, and N. R. Newbury, "High-stability transfer of an optical frequency over long fiber-optic links," J. Opt. Soc. Am. B **25**, 1284 (2008).
21. O. Lopez, A. Haboucha, F. Kéfélian, *et al.*, "Cascaded multiplexed optical link on a telecommunication network for frequency dissemination," Opt. Express **18**, 16849 (2010).
22. S. Droste, F. Ozimek, Th. Udem, *et al.*, "Optical-frequency transfer over a single-span 1840 km fiber link," Phys. Rev. Lett. **111**, 110801 (2013).
23. S. J. Guan, Y. S. Zhang, J. L. Zheng, *et al.*, "Modulation bandwidth enhancement and frequency chirp suppression in two-section DFB laser," J. Lightwave Technol. **40**, 7383 (2022).